Isotopic Mass Fractionation of Solar Wind: Evidence from Fast and Slow Solar Wind Collected by the Genesis mission

8 authors, including:

Veronika Heber
Paul Scherrer Institut
98 PUBLICATIONS   945 CITATIONS

Heinrich Baur
ETH Zurich
225 PUBLICATIONS   3,931 CITATIONS

Kevin Mckeegan
University of California, Los Angeles
308 PUBLICATIONS   8,319 CITATIONS

D. B. Reisenfeld
University of Montana
214 PUBLICATIONS   3,273 CITATIONS

ISOTOPIC MASS FRACTIONATION OF SOLAR WIND: EVIDENCE FROM FAST AND SLOW SOLAR WIND COLLECTED BY THE *GENESIS* MISSION

VERONIKA S. HEBER[1,2], HEINRICH BAUR[1], PETER BOCHSLER[3,4], KEVIN D. MCKEEGAN[2], MARCIA NEUGEBAUER[5],
DANIEL B. REISENFELD[6], RAINER WIELER[1], AND ROGER C. WIENS[7]

[1] Institute for Geochemistry and Petrology, ETH Zurich, Clausiusstrasse 25, CH-8092 Zurich, Switzerland
[2] Department of Earth and Space Sciences, University of California Los Angeles, 595 Charles Young Drive East,
Box 951567, Los Angeles, CA 90095-1567, USA heber@ess.ucla.edu
[3] Physikalisches Institut, Universität Bern, Sidlerstasse 5, CH-3012 Bern, Switzerland
[4] Space Science Center and Department of Physics, University of New Hampshire, Durham, NH 03824, USA
[5] Lunar and Planetary Laboratory, University of Arizona, Tucson, AZ 85721-0092, USA
[6] Department of Physics & Astronomy, University of Montana, Missoula, MT 59812, USA
[7] Los Alamos National Laboratory, Los Alamos, NM 87545, USA.

ABSTRACT

NASA's *Genesis* space mission returned samples of solar wind collected over $\sim$2.3 years. We present elemental and isotopic compositions of He, Ne, and Ar analyzed in diamond-like carbon targets from the slow and fast solar wind collectors to investigate isotopic fractionation processes during solar wind formation. The solar wind provides information on the isotopic composition for most volatile elements for the solar atmosphere, the bulk Sun and, hence, on the solar nebula from which it formed 4.6 Ga ago. Our data reveal a heavy isotope depletion in the slow solar wind compared to the fast wind composition by 63.1 ± 2.1‰ for He, 4.2 ± 0.5‰ amu^{-1} for Ne and 2.6 ± 0.5‰ amu^{-1} for Ar. The three Ne isotopes suggest that isotopic fractionation processes between fast and slow solar wind are mass dependent. The He/H ratios of the collected slow and fast solar wind samples are 0.0344 and 0.0406, respectively. The inefficient Coulomb drag model reproduces the measured isotopic fractionation between fast and slow wind. Therefore, we apply this model to infer the photospheric isotopic composition of He, Ne, and Ar from our solar wind data. We also compare the isotopic composition of oxygen and nitrogen measured in the solar wind with values of early solar system condensates, probably representing solar nebula composition. We interpret the differences between these samples as being due to isotopic fractionation during solar wind formation. For both elements, the magnitude and sign of the observed differences are in good agreement with the values predicted by the inefficient Coulomb drag model.

Key words: Methods: analytical – Methods: laboratory – solar wind – Space vehicles – Sun: abundances – Sun: photosphere

Online-only material: color figures

1. INTRODUCTION

NASA's *Genesis* solar wind sample return mission was launched in 2001 to obtain samples of solar wind that could be analyzed with high precision in laboratories, particularly for isotope ratios, with the ultimate goal of determining the composition of the Sun and the solar nebula from which it was formed (Burnett et al. 2003). A fundamental premise motivating the mission was that the isotopic composition of the solar wind is representative of the outer convective zone (OCZ) of the Sun, which closely preserves the average isotopic composition of the primitive solar nebula. Known exceptions are the D/H and ^{7}Li/^{6}Li ratios, both affected by nuclear burning during the pre-main-sequence phase of the Sun (e.g., Geiss & Reeves 1972; Bochsler 2000). Additionally, elements heavier than H are possibly affected by gravitational settling associated with a potential ^{3}He/^{4}He enrichment in the OCZ on the order of about 30‰ over the history of the Sun (Bochsler 2000; Turcotte & Wimmer-Schweingruber 2002). Minor differences could also be expected due to isotopic fractionation processes upon ionization and acceleration of the solar wind. The latter effects are the topic of this paper.

The solar wind is about the only source of information regarding the isotopic compositions of highly volatile elements (e.g., oxygen, nitrogen, and noble gases) in the Sun and hence in the primordial solar nebula, apart from atmospheres of giant planets and maybe comets. The compositions of the latter, however, cannot be analyzed in situ with the high precision required to allow the detection of distinct differences between solar system objects in most cases. Similarly, isotopic compositions inferred from molecular absorption lines in relatively cool regions of the solar atmosphere are likely to suffer from large systematic errors (see discussion in Asplund et al. 2009). The usual approach of resorting to primitive meteorites also fails, since the traces of nitrogen and noble gases in meteorites are generally not derived from a solar source. Also, the complex oxygen isotope systematic in meteorites inhibits a straightforward derivation of the solar nebula oxygen composition (Clayton 2003). Information on the isotopic composition of reactive highly volatile elements can, in principle, be derived from unaltered solar nebula condensates as these may have incorporated the prevailing isotopic composition of the respective element, e.g., O in refractory inclusions (e.g., Liu et al. 2009) or N in osbornite (Meibom et al. 2007). However, deciding exactly which samples are appropriate is model dependent. Furthermore, the solar nebula might not have been well mixed, exhibiting a non-uniform composition during the condensation of these samples. The bulk solar nebula isotopic composition for most highly volatile elements is thus best deduced from solar wind data. Therefore, a quantitative understanding of processes fractionating isotopic and elemental

abundances during solar wind formation is a necessary key ingredient for modeling the origin of the solar system.

In situ spacecraft measurements detected clear differences in the He isotopic composition between fast and slow solar wind (Bodmer & Bochsler 1998b; Gloeckler & Geiss 2000) which were interpreted (Bürgi & Geiss 1986; Bodmer & Bochsler 1998a, 2000) as being due to processes occurring during the acceleration of the solar wind. A correlation was also detected between He isotopic composition and the He/Ne ratio (see Bochsler 2007a) in averaged data from individual aluminum foil experiments exposed to the solar wind during the *Apollo* missions (Geiss et al. 1972; Geiss et al. 2004), although solar wind collection times were random and not intended to sample particular regimes in these experiments.

A combined analysis of in situ measured Ne, Si, and Mg revealed a weak depletion of the heavy isotope in the slow solar wind by $14 \pm 13\text{‰ amu}^{-1}$ (Kallenbach et al. 1998b). Apart from this study, however, differences in isotopic composition between fast and slow solar wind could not be detected for heavier elements by in situ analysis (Boschler et al. 1997; Weygand et al. 2001). Also, isotopic composition data obtained in situ on non-volatile elements in the bulk solar wind have uncertainties that are too large to accurately characterize isotopic fractionation between the Sun (as represented by the terrestrial isotopic composition) and solar wind, although upper limits were reported (e.g. Kallenbach et al. 1998a; Wimmer-Schweingruber et al. 1998; Karrer et al. 2007).

In this work we present He, Ne, and Ar isotopic and elemental abundances of the slow and fast solar wind collected separately by the NASA *Genesis* spacecraft. Our data allow for the first time a comprehensive characterization of the isotopic fractionation of solar wind over a significant mass range. We investigate currently available theoretical models for isotopic fractionation processes (Bodmer & Bochsler 1998a, 2000; Gloeckler & Geiss 2000) to draw conclusions on photospheric and thus solar nebula isotopic compositions measured in the solar wind.

2. *GENESIS* SOLAR WIND REGIME SELECTION

Genesis collected solar wind ions for 2.3 years from 2001 November to 2004 April (at and after the maximum of solar cycle 23) in a halo orbit around the Lagrange point L1 (Burnett et al. 2003; Burnett & Team 2011). Besides a collector array that was continuously exposed, thus capturing a bulk solar wind sample, a mechanism was employed that allowed collection of specific main solar wind regimes: fast wind, slow wind, and wind from coronal mass ejections (CMEs), on separately deployed collectors (Neugebauer et al. 2003).

The deployment of the regime arrays was controlled by an algorithm (Neugebauer et al. 2003) that processed in real-time data from the Genesis ion and electron monitors (GIM, GEM) (Barraclough et al. 2003). Solar wind composition correlates with solar wind speed. Generally, the fast solar wind originates in coronal holes, and the slow wind originates at the boundaries of near-equatorial streamer belts. The regime selection algorithm did not simply use a single speed set point to differentiate between fast and slow wind, but it partially compensated for the fact that the solar wind evolves as it propagates through interplanetary space. This evolution can obscure the source signature in that (1) originally slow solar wind just ahead of higher speed wind is accelerated as the faster wind compresses it and (2) originally fast solar wind running away from slower wind will decelerate into the resulting pressure rarefaction. The algorithm accounted for this through the use of "hysteresis" such

that when a slow-to-fast transition occurs, the speed set point for retracting the slow wind collector and deploying the fast wind collector was set to 525 km s^{-1}; when a fast-to-slow transition occurs, the set point for retracting the fast wind collector and deploying the slow wind collector was set to 425 km s^{-1}. Thus, although there is a common speed range to which both collectors were exposed, they captured different compositions (Reisenfeld et al. 2007). Transient CME events were recognized by either an He/H ratio of >0.06, counterstreaming, suprathermal electrons or by a reduced proton temperature. Details regarding the regime selection algorithm are given in Neugebauer et al. (2003). Particular attention was paid to avoid contributions from CME matter to the fast and slow solar wind collection (Neugebauer et al. 2003). This was important as the fast solar wind is considered to represent the least fractionated solar wind type, whereas CMEs on the other hand, are variable, and potentially also anomalously composed (e.g., Wurz et al. 2000; Zurbuchen et al. 2003). Total exposure times of the bulk solar wind collectors were 852.83 days. The three other collectors sampled mutually exclusive 333.67 days (slow wind), 313.01 days (fast wind), and 193.25 days (CME; Reisenfeld et al. 2007). The spacecraft was in safe mode for a period of 11.25 days during which the bulk collector and, unintended but fortunate, the CME regime collector was exposed even though no monitoring of the solar wind was being performed.

Reisenfeld et al. (2007) tested the success of the regime selection algorithm post-flight, by discriminating elemental abundances (C, O, Mg, Fe) measured by the SWICS instrument on board the *Advanced Composition Explorer* (*ACE*) at the same period as the *Genesis* operation using the *Genesis* regime selection algorithm. All elements showed speed-dependent abundance variations and CMEs showed a distinctly different composition relative to slow and fast solar wind for some elements. Furthermore, a post-flight analysis of solar wind data from the *Genesis* and *ACE* electron and ion monitors was performed to verify the autonomous identification of CMEs by *Genesis*. The conservative nature of the algorithm was deemed particularly important to ensure that the slow and fast solar wind regime collectors were not contaminated by CME material. This was in fact the case: the post-flight analysis based on a comparison with *ACE*/SWICS data showed that only 4% of the implanted ions in the slow solar wind collector and 1.3% in the fast solar wind collector stem from CME material.

3. ANALYTICAL PROCEDURE

3.1. Samples and Noble Gas Extraction

Each *Genesis* collector array was equipped with a variety of ultrapure targets (Jurewicz et al. 2003). For this work, we chose amorphous diamond-like carbon film deposited on a silicon substrate target (abbreviated here as DOS). The most important properties making DOS an ideal solar wind collector material are its very low diffusivity for trapped noble gases (see diffusion experiment in Heber et al. 2009), resulting in a quantitative retention of implanted solar wind noble gases, and the low atomic mass of carbon, minimizing backscatter loss, and related corrections. The selected target materials and sample preparation details are given in Heber et al. (2009). Target fragments in the size range of 10–40 mm^2 (Figure 1) were analyzed for He, Ne, and Ar at ETH Zurich. In this work we discuss the results of the analysis of the slow, fast, and bulk solar wind regime samples (see Tables 3 and 4 for respective NASA codes).
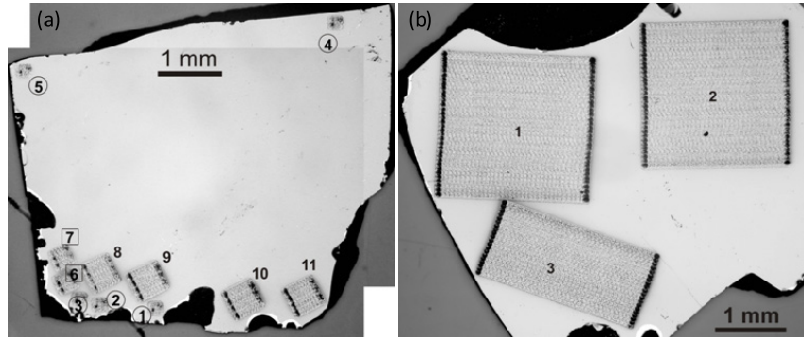
Figure 1. Photomicrographs of analyzed DOS collector-target fragments. (a) Example of ablation raster sizes required for He and Ne analysis using the high-sensitivity mass spectrometer (60256, slow solar wind); numbers in circles represent He isotope, numbers in squares ^{4}He/^{20}Ne, and numbers without circles and squares Ne isotope analyses. (b) Raster sizes required for Ar analysis using the Albatros mass spectrometer (60257, slow solar wind).

Prior to analysis, all samples were baked at 100°C for 40 hr in vacuum to remove adsorbed atmospheric gases. A pulsed 213 nm UV laser beam was rastered over a rectangular area (Figure 1) and quantitatively released the implanted solar noble gases trapped in the near-surface layer of the target. The thickness of the ablated layer was on the order of 1 μm. Laser extraction conditions resemble those given for He, Ne, and Ar in Heber et al. (2009). The ablated areas were adjusted to match gas amounts released from the different solar wind regime samples. Typical raster sizes were 0.02–0.05 mm^2 for He isotope analyses, 0.1–0.3 mm^2 for Ne isotope analyses, and 0.04–0.1 mm^2 for the ^{4}He/^{20}Ne ratio analysis using the high-sensitivity mass spectrometer (Figure 1(a)). Typical raster sizes for Ar with the conventional mass spectrometer were 4 mm^2 for the regime and 1–2 mm^2 for the bulk samples (Figure 1(b)). Solar wind noble gas fluences were determined from the gas amount released and the area of each raster pit measured on a photomicrograph.

3.2. Noble Gas Mass Spectrometry

Data were obtained using two different noble gas mass spectrometer systems. The analytical procedures and conditions adopted for the conventional (Albatros) and high-sensitivity (Tom) mass spectrometers are described in detail in Heber et al. (2009) and Heber et al. (2011), respectively. Tom is equipped with a molecular drag compressor that concentrates the gas in the ionization chamber (Baur 1999); factors of 34 to 80 times higher sensitivity for He and Ne, respectively, can be achieved compared to the Albatros mass spectrometer. Tom was used for He and Ne analyses. Because we expected compositional differences between the different regimes to be very small, we adopted a standard-sample bracketing technique for He and Ne. This technique is frequently used for high-precision isotope analyses when very small differences need to be detected (e.g., Albarède & Beard 2004). In our protocol, an analysis of the regime target, the "sample," was always measured in between two analyses of a bulk solar wind target, the "standard." This comparison between "sample" and "standard" allowed a precise determination of any small deviation in isotopic composition of a respective regime sample from the bulk solar wind composition by correcting for potential sensitivity variations of the mass spectrometer.

This high-sensitivity mass spectrometer allowed high-precision analyses consuming only small target areas, which permitted us to analyze the He isotopes, the Ne isotopes, and the He/Ne ratio in separate runs, thereby minimizing the time that elapsed between two bracketing analyses of the standard.

Thus, the duration of an analysis was also minimized by this procedure, despite measuring the minor isotope with longer integration times, e.g., 60 s for ^{3}He and ^{21}Ne. An important advantage is that this ensured a reliable extrapolation of isotope signals back to the gas inlet time. Our statistical counting errors were less than 0.1% for all isotopes except for ^{21}Ne for which statistical errors were $\leqslant 0.3\%$.

After gas extraction and removal of non-noble gas components, He was directly admitted to the mass spectrometer. Both He isotopes were measured simultaneously, ^{3}He on an electron multiplier and ^{4}He in a Faraday cup. For the Ne isotope analysis, after gas release, Ne was first frozen onto a cryogenic trap held at 12.7 K for 15 minutes to concentrate the Ne gas into a small volume and also to pump off the He fraction (with the volume containing the frozen Ne being closed). As this mass spectrometer is frequently used for low-concentration terrestrial ^{3}He analyses, this procedure avoided contamination of the spectrometer with comparatively large amounts of solar wind ^{3}He. Neon was then released from the cryotrap at 50 K and directly admitted to the mass spectrometer (see for analytical details Heber et al. 2011). For the ^{4}He/^{20}Ne ratio analysis, after purification, the sample gas was directly admitted to the mass spectrometer. Ne isotopes and the ^{4}He/^{20}Ne ratio were measured by magnetic field peak-jumping using a single detector (electron multiplier for Ne and Faraday cup for He).

Albatros is equipped with a conventional Baur–Signer source (Baur 1980) and was required for the Ar analysis because the high ion pumping speed of Tom inhibits the analysis of this element. He and Ne were also analyzed in these runs to determine the Ne/Ar elemental ratio and the noble gas fluences. Larger sample area consumption (Figure 1(b); due to the lower mass spectrometer sensitivity and the lower Ar amount in the solar wind) and the longer time required for extraction, gas separation, and analysis prevented a bracketing of regime samples with bulk samples. Thus, a bulk solar wind analysis was carried out at the beginning and the end of each day with 1–3 regime samples analyzed in-between. The Ar sensitivity of this mass spectrometer varied by less than 0.3% over several days.

The sensitivity and mass discrimination of both mass spectrometers were regularly determined by analyzing known amounts of standard gases with known isotopic composition (Heber et al. 2009).

3.3. Interferences and Blank Correction

Possible interferences of HD and ^{3}H on ^{3}He, and H$_2$^{18}O on ^{20}Ne could be resolved in both mass spectrometers. Noble
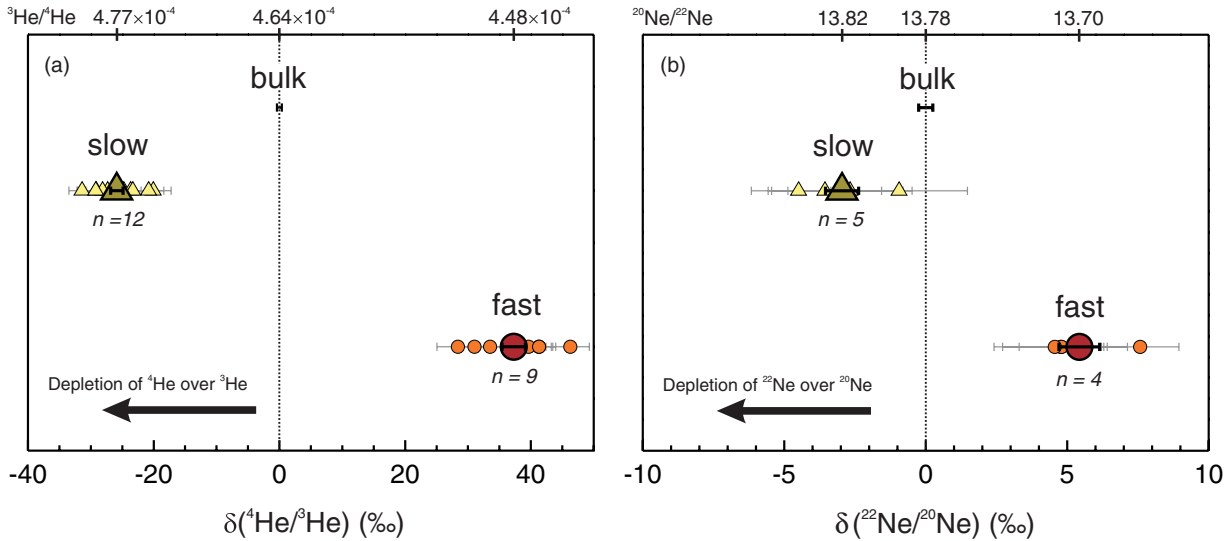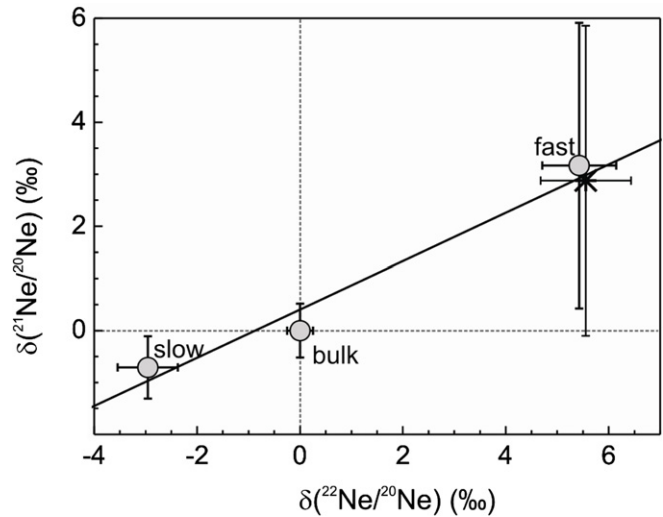
Figure 2. (a) Helium and (b) Ne isotopic compositions of the solar wind regimes expressed as permil deviations relative to the bulk solar wind composition (Heber et al 2009). Here and in Figure 3, small symbols represent n single measurements and large symbols represent the mean value (Table 3). Negative values indicate heavy isotope depletion. The mean heavy isotope depletions in the slow relative to the fast solar wind are $63.1 \pm 2.1‰$ amu^{-1} for He and $4.2 \pm 0.5‰$ amu^{-1} for Ne.
(A color version of this figure is available in the online journal.)
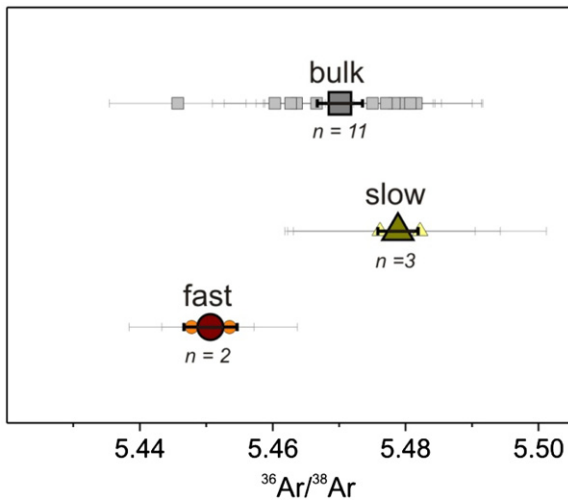
Figure 3. Argon isotopic composition of the fast and slow solar wind regimes as well as the bulk solar wind composition. The slow solar wind is also depleted in the heavy Ar isotope, by $2.6 \pm 0.5‰$ amu^{-1} relative to the fast solar wind.
(A color version of this figure is available in the online journal.)

Figure 4. Mean measured Ne isotopic compositions of each of the solar wind regimes are plotted as permil deviation to the bulk solar wind in a three-isotope plot. The preliminary CME Ne isotopic composition (Heber et al. 2008) is shown by the asterisk and corresponding error bars near the fast solar wind composition. Error bars are 1σ standard error (Table 3). The fit through all data is represented by the solid line. The slope of the fit (0.464 ± 0.053) is within uncertainty consistent with a mass-dependent fractionation. The slope of a fit only through fast and slow solar wind, thus excluding CME and CME-influenced bulk solar wind, is with 0.463 similar to the all-data-fit.

gas atoms are ionized by electron impact. A relatively low electron acceleration voltage of 45 eV (Albatros) and 40 eV (Tom), respectively, was used to minimize interferences from doubly charged ^{40}Ar and CO_2. Their relative contributions to the ^{20}Ne and ^{22}Ne samples were $\sim 0.02\%$ and $\sim 0.04\%$ (Tom) and 0.0004% and 0.09% (Albatros), respectively. The hydrogen level in both mass spectrometers was low and did not vary between sample and blank analyses. Thus, the additional hydrogen from the solar wind was quantitatively removed from the sample gas by Ti + Zr and Al + Zr getters in both gas-purification systems. Therefore, we exclude that detectable amounts of ^{20}NeH were interfering on ^{21}Ne during sample analysis, as discussed in detail in Heber et al. (2009).

All data were corrected for the procedural blank, i.e., the procedure that mimics the sample analysis conditions without applying the laser. The material blanks, i.e., indigenous He,

Ne, and Ar amounts in the DOS material, are negligible as demonstrated in Heber et al. (2009). Procedural blanks were low and nearly constant. In the high-sensitivity spectrometer, blank contributions were $<0.1\%$ for both He isotopes and $\leqslant 0.3\%$ for Ne isotopes. A somewhat higher ^{20}Ne blank averaging 0.8% was observed during the $^{4}He/^{20}Ne$ measurement due to the lower amounts of Ne admitted. For the Albatros mass spectrometer the blank contribution to both He isotopes was $<0.05\%$, to Ne $\leqslant$ 0.1%, and to $^{36,38}Ar \leqslant 1\%$. Correcting the two Ar isotopes in the solar wind by blank subtraction or by assuming all ^{40}Ar in a sample run to be atmospheric led to identical $^{36}Ar/^{38}Ar$ ratios.

Table 1
SRIM-based Backscatter Correction for ^{4}He and
^{3}He/^{4}He and ^{4}He/^{20}Ne Ratios

Solar Wind Regimes	^{4}He	^{3}He/^{4}He	^{4}He/^{20}Ne
	(%)		
Bulk	1.17	1.0080	1.0118
Fast	0.75	1.0053	1.0076
Slow	1.60	1.0108	1.0162

Notes. Backscatter loss of ^{4}He is given in%. Measured ^{3}He/^{4}He and ^{4}He/^{20}Ne ratios were corrected by multiplication with the factors given in third and fourth columns.

4. RESULTS

4.1. Correction for Backscatter Loss

Backscatter loss was estimated using the Stopping and Range of Ions in Matter (SRIM) code of Ziegler (2004). We simulated implantation of ^{3}He and ^{4}He into carbon of a density of 2.25 g cm^{-3} for 21 solar wind speeds ranging from 200 to 1200 km s^{-1} (each with 10^5 ions) and for ^{20}Ne and ^{22}Ne for 4 speeds between 250 and 400 km s^{-1}. The simulated backscatter loss is similar for carbon with densities between 2.25 g cm^{-3} and 3.26 g cm^{-3}, the latter representing one of the highest densities of diamond-like carbon films, (Shamsa et al. 2006). Heber et al. (2009) showed that SRIM predicts backscatter losses reliably for implantation of light noble gas ions with normal incidence into carbon. Backscatter loss factors were weighted for each regime according to the respective solar wind He speed distribution as measured by the SWICS instrument on board *ACE* over the solar wind collection period of *Genesis*. All data involving He (^{4}He flux, ^{3}He/^{4}He, ^{4}He/^{20}Ne) are corrected for minor backscatter loss (see Table 1). Heavier mass ions are less affected by backscattering. The maximum simulated loss of ^{20}Ne backscattered from carbon in the DOS target is only 0.007% for a very low solar wind speed of 250 km s^{-1}. Therefore, Ne was not measurably affected by backscatter losses and thus no corrections were applied. The same is true for Ar.

4.2. Data Evaluation

A summary of the isotopic and elemental composition of the slow and the fast solar wind is given in Table 2; this table also includes the mean bulk solar wind composition published in Heber et al. (2009) for comparison. Tables 3 and 4 show the individual data from the high-sensitivity and Albatros mass spectrometer measurements, respectively.

Standard-sample bracketing data reduction and errors. For the data obtained by the high-sensitivity system, we calculated the permil deviation (δ) of each regime sample from the mean of its two bracketing bulk solar wind targets ("standard") according to the equation

$$\left(\frac{R_{\text{sample}}}{\bar{R}_{\text{standard}}} - 1 \right) \times 1000 = \delta(‰), \tag{1}$$

where R stands for a ratio of a heavy to a light isotope of an element. Data are given in Table 3 and shown in Figure 2. Uncertainties of the single δ-values are 1σ and include analytical uncertainties of the regime and the adjacent bulk solar wind measurements as well as the error due to blank correction. Arithmetic means were calculated from n replica δ-values; the reported error is the 1σ-standard error of the mean. Finally,

the absolute isotopic and elemental composition of each solar wind regime (Table 2) was calculated from the δ-values and the respective bulk solar wind composition given in Table 2 (Heber et al. 2009).

Albatros mass spectrometer analysis. He, Ne, and Ar concentrations were corrected for blank and mass spectrometer sensitivity, the isotopic ratios for blank and instrumental mass discrimination. Uncertainties of single data points are 1σ. Single bulk solar wind data are listed in Heber et al. (2009), the single regime data in Table 4, and for Ar the isotopic composition is shown in Figure 3. The permil deviation of the Ar isotopic composition of the regimes in Table 2 was calculated from the mean deviation of a respective regime relative to the bulk composition.

4.3. Isotopic Composition of the Fast and Slow Solar Wind

The slow solar wind shows a depletion of the heavy isotopes for all three elements, He, Ne, and Ar, relative to the fast solar wind. It is most pronounced in He with a depletion of ^{4}He relative to ^{3}He by $63.1 \pm 2.1‰$. Depletion factors decrease with increasing elemental mass: $4.2 \pm 0.5‰$ amu^{-1} for Ne and $2.6 \pm 0.5‰$ amu^{-1} for Ar (Figures 2 and 3). Both techniques, the conventional mass spectrometer analysis and the standard-sample bracketing with the high-sensitivity mass spectrometer, result in identical He and Ne isotopic compositions within uncertainties. Note that the isotopic composition of the third solar wind regime separately collected on *Genesis*, the CMEs, is indistinguishable from the bulk solar wind for He and Ar and similar to the fast solar wind composition for Ne. Mass balance calculations verify that the fluence-weighted mean of slow, fast, and CME isotopic compositions is equal to the respective bulk solar wind isotopic composition within $0.6‰$ for ^{3}He/^{4}He, ^{21}Ne/^{22}Ne, and ^{36}Ar/^{38}Ar, and $2.2‰$ for ^{20}Ne/^{22}Ne ratios. It is beyond the scope of this paper, however, to discuss in detail the results obtained for the CME regime sample here. CMEs differ from the solar wind regimes covered in this work because of their transient character and anomalous elemental compositions. Preliminary CME data are given in Heber et al. (2008) and final data will be published elsewhere.

The three Ne isotopes allow us to investigate whether the isotopic fractionation is mass dependent. So far, Ne is the only element for which more than two isotopes of solar wind origin were measured in the regime targets (Heber et al. 2009; Vogel et al. 2011a). Figure 4 shows the Ne isotopic composition in the three-isotope plot. The slope of the line fitted through all data (0.464 ± 0.053) is consistent with a mass-dependent fractionation line of slope ~ 0.5 within uncertainties. A fit laid through fast and slow solar wind compositions only, thus excluding CME and CME-influenced bulk composition, results in a similar slope of 0.463. Note that both the fast and the slow solar wind samples contain at most minute amounts of CME matter (1.3% and 4%, respectively). Thus, our data show that the processes responsible for isotopic fractionation between fast and slow solar wind are to first-order linearly mass dependent. This finding is, for example, crucial to understand how the solar photospheric and thus the solar nebula oxygen isotopic composition has to be extrapolated from the composition measured in the solar wind (McKeegan et al. 2011).

4.4. Fluences and the Elemental Composition of the Fast and Slow Solar Wind

Solar wind fluxes of He, Ne, and Ar are given in Table 2. Average He, Ne, and Ar fluxes were determined from the

Table 2
The Isotopic and Elemental Compositions of Slow and Fast Solar Wind as Measured in *Genesis* Samples

Solar Wind Regime	Exposure (days)	H Flux[a] ($\times 10^8$)	^{4}He/H	^{4}He Flux ($\times 10^7$)	^{20}Ne Flux ($\times 10^4$)	^{36}Ar Flux ($\times 10^2$)	^{3}He/^{4}He ($\times 10^{-4}$)	^{20}Ne/^{22}Ne	^{21}Ne/^{22}Ne	^{36}Ar/^{38}Ar	^{4}He/^{20}Ne	^{20}Ne/^{36}Ar
Bulk	852.83	2.80	0.0402	1.125(3)	1.716(7)	4.07(2)	4.645(8)	13.777(10)	0.03289(7)	5.470(3)	655.7(1.4)	42.15(08)
Fast	313.01	2.37	0.0406	0.960(2)	1.529(7)	3.75(4)	4.478(11)	13.703(14)	0.03282(12)	5.451(4)	627.9(2.8)	40.78(50)
Slow	333.67	3.17	0.0344	1.093(4)	1.708(9)	4.10(2)	4.768(9)	13.818(13)	0.03297(8)	5.479(3)	640.2(1.2)	41.67(11)
		Depletion of the heavy isotope in slow relative to fast solar wind					63.1 ± 21(‰)	4.19 ± 0.46 (‰ amu^{-1})		2.58 ± 0.46 (‰ amu^{-1})		

Notes. H fluxes are from the *Genesis* Ion Monitor (GIM; Reisenfeld et al. 2007). He/H ratios were calculated from GIM H fluences and He fluences measured in DOS. Bulk solar wind values are published in Heber et al. (2009) and are given here for completeness. Single data and type and source of errors are given in Table 3 for He and Ne isotopic composition and in Table 4 for Ar isotopic composition, elemental fluxes, ^{4}He/^{20}Ne, ^{20}Ne/^{36}Ar. Errors are 1σ. The permil depletions of heavy isotopes were calculated by adding the respective mean permil deviations of the fast and slow to the bulk solar wind (see Table 3); errors were quadratically added. Here and Tables 3 and 4: numbers in parentheses represent the uncertainty in units of the least significant digit(s).
[a] Fluxes are given in atoms cm^{-2} s^{-1}.

Table 3
Measured Fast and Slow Solar Wind of the He and Ne Isotopic Composition and the ^{20}Ne/^{4}He Ratio (Standard-sample Bracketing Technique)

SLOW SOLAR WIND			FAST SOLAR WIND		
Lab code	$\delta(^{4}$He/^{3}He) (‰)		Lab code	$\delta(^{4}$He/^{3}He) (‰)	
vh,09,06 - 1	−24.7(2.7)		vh,01,07 - 1	*52.4(2.5)*	
2	−20.1(2.8)		2	*29.3(3.4)*	
3	−20.8(2.4)		3	41.3(2.2)	
4	−23.7(2.8)		4	33.5(2.3)	
5	−23.3(2.9)		5	36.4(2.4)	
12	−29.1(3.1)		6	37.7(2.1)	
13	−27.3(2.3)		10	46.3(3.0)	
14	−26.4(2.5)		11	39.6(2.8)	
16	*−32.9(2.1)*		12	31.0(2.8)	
17	−26.2(2.8)		13	28.4(3.3)	
18	−28.1(2.7)		14	41.3(2.6)	
19	−31.4(2.1)				
20	−29.2(2.8)				
Mean	**−25.9 (1.0)**		Mean	**37.3(1.9)**	
Absolute mean ^{3}He/^{4}He	**(4.768 ± 0.009)×10^{-4}**		**(4.478 ± 0.011)×10^{-4}**		
	$\delta(^{22}$Ne/^{20}Ne) (‰)	$\delta(^{21}$Ne/^{20}Ne) (‰)		$\delta(^{22}$Ne/^{20}Ne) (‰)	$\delta(^{21}$Ne/^{20}Ne) (‰)
vh,09,06 - 8	−3.1(2.3)	−2.0(4.8)	Vh,01,07 -21	7.6(1.4)	10.4(4.9)
9	−2.7(2.2)	−1.8(3.5)	22	4.8(2.4)	3.0(3.9)
10	−0.9(2.4)	0.7(3.7)	23	4.8(1.5)	2.1(2.8)
11	*−3.0(2.2)*	*−2.5(3.8)*	24	4.6(1.8)	-2.9(3.7)
27	−3.6(2.0)	0.8(2.6)			
28	−4.5(1.7)	−1.2(3.3)			
Mean	**−3.0(0.6)**	**−0.71(0.60)**	Mean	**5.4(0.7)**	**3.2(2.7)**
Absolute mean ^{20}Ne/^{22}Ne	**13.818 ± 0.013**		**13.703 ± 0.014**		
^{21}Ne/^{22}Ne	**0.03297 ± 0.00008**		**0.03282 ± 0.00012**		
	$\delta(^{20}$Ne/^{4}He) (‰)			$\delta(^{20}$Ne/^{4}He) (‰)	
vh,09,06 - 6	43.0(4.0)		vh,01,07 - 7	23.6(4.1)	
7	45.3(3.3)		8	29.6(3.3)	
15	46.4(4.2)		9	45.2(3.9)	
21	37.7(2.9)		15	30.4(3.8)	
22	27.6(3.5)		16	33.8(3.4)	
23	35.7(2.9)		17	45.6(3.0)	
24	37.1(3.2)		18	21.4(2.8)	
25	40.2(3.5)		19	30.4(3.6)	
			20	27.3(3.5)	
Mean	**39.1(2.1)**		Mean	**31.9(2.8)**	
Absolute mean ^{4}He/^{20}Ne	**631.0 ± 1.9**		**635.4 ± 2.3**		

Notes. Permil deviations are relative to measured bulk solar wind measured values; see Section 4.2 for explanation. Error of single data is 1σ. Error of the mean permil deviation values is the 1σ standard error. The absolute mean ratios include the error of the bulk sample. ^{4}He, ^{3}He/^{4}He, and ^{4}He/^{20}Ne data are backscatter corrected. Data in italics are somewhat corrupted due to laser ablation problems and are not included in the mean. NASA codes of samples used: bulk solar wind: 60253 (fragment size 24.0 mm^2, lab code vh,07,06); 60067 (fragment size 15.5 mm^2, lab name vh,04,06); slow solar wind: 60256 (fragment size 24.3 mm^2, lab code vh,09,06); fast solar wind: 60244 (fragment size 12.6 mm^2, lab code vh,01,07).

measured noble gas abundances divided by the extracted area on the target and the integrated time that the respective solar wind regime collector was deployed. We used data from the Albatros mass spectrometer to determine the fluences as the large rastered areas (required to extract sufficient solar wind Ar) facilitated a precise area measurement using photomicrographs (Heber et al. 2009). Helium, Ne, and Ar fluxes are about 14% (He), 12% (Ne), and 10% (Ar) higher in the slow relative to the fast solar wind. However, in contrast to our results, the in situ measured oxygen flux is not enhanced in the slow relative to the fast solar wind (von Steiger et al. 2010), although oxygen could be expected to behave similarly as the minor ions Ne and Ar, i.e., should show a similarly enriched flux in slow solar wind.

We also observe a 34% higher proton flux in the slow relative to the fast solar wind in agreement with in situ data (see below).

The abundances of He, Ne, and Ar relative to H (see below) are lower in the slow solar wind than in the fast wind by 15% (He), 17% (Ne), and 18% (Ar). Also, in situ measurements yielded lower He/H ratios in the slow solar wind (Kasper et al. 2007).

He/Ne and Ne/Ar ratios were calculated from the measured fluences (Tables 2 and 4). The ^{4}He/^{20}Ne and the ^{20}Ne/^{36}Ar ratios indicate a slight enrichment of the respective light element in the slow compared to the fast solar wind by 20 ± 5‰ and 22 ± 13‰, respectively. This conclusion for the ^{4}He/^{20}Ne ratio is, however, preliminary, as the standard-sample bracketing method

Table 4
He, Ne, and Ar Fluences and the Ar Isotopic Composition Measured in Solar Wind Regimes with the Albatros Mass Spectrometer

Solar Wind Regime	No. of Analysis	Rastered Area (mm^2)	^{4}He ($\times 10^{14}$)	^{20}Ne ($\times 10^{11}$)	^{36}Ar ($\times 10^{10}$)	^{36}Ar/^{38}Ar	^{4}He/^{20}Ne	^{20}Ne/^{36}Ar
Slow	1	4.53	3.14(1)	4.90(4)	1.174(4)	5.478(16)	641(6)	41.8(4)
	2	4.36	3.15(1)	4.91(4)	1.182(4)	5.482(19)	641(6)	41.6(4)
	3	2.62	3.163(2)	4.95(2)	1.188(5)	5.476(14)	639(3)	41.7(3)
	Mean		**3.15(1)**	**4.92(3)**	**1.181(7)**	**5.479(3)**	**640.2(1.2)**	**41.67(11)**
Fast	1	4.25	2.589(2)	4.13(2)	1.026(6)	5.453(10)	628(2)	40.2(3)
	2	4.20	2.598(2)	4.16(2)	1.009(4)	5.448(9)	625(2)	41.2(2)
	3	4.22	2.600(1)	4.12(2)	1.006(4)	5.406(16)[a]	631(3)	41.0(3)
	Mean		**2.596(6)**	**4.13(2)**	**1.01(1)**	**5.451(4)**	**627.9(2.8)**	**40.78(50)**

Notes. Single data of bulk regime are given in Heber et al. (2009). Fluences are given in atoms cm^{-2}. He and the ^{4}He/^{20}Ne ratio are corrected for backscatter loss. Errors of single abundances are 1σ and include statistical error, error due to blank reduction and sensitivity variability; isotope ratio errors include the statistical error, error due to blank reduction and mass discrimination. Error of the mean values (appearing in bold) is 1σ standard deviation. NASA codes of samples used: slow solar wind: 60257 (fragment size 30.7 mm^2, lab code vh,08,07); fast solar wind: 41092 (fragment size 48.5 mm^2, lab code vh,21,07).
[a] Ar analysis was adopted after four cycles, thus the Ar isotopic ratio is corrupted and therefore not included in the mean.

resulted in the opposite trend—a slight depletion in ^{4}He over ^{20}Ne by 7 ± 4‰ relative to fast solar wind (Table 4). We do not know the reason for this discrepancy and whether the standard-sample bracketing method, otherwise very precise for isotope ratios, could introduce systematic biases for elemental ratios. On the other hand, the ^{4}He/^{20}Ne ratios are the same within 3σ uncertainties for the slow and fast solar wind. In the future, more precise measurements on *Genesis* targets with emphasis on the elemental ratios in slow and fast solar wind should be carried out to ascertain whether any real differences in elemental composition are resolvable. Overall, the measured He, Ne, and Ar elemental fractionations in the fast and slow solar wind as collected by *Genesis* are surprisingly small, at most about 40‰ (He/Ar), which is in strong contrast to the observed isotopic fractionation of, for example, He of 63‰.

The H fluences for the solar wind regimes were obtained by the GIM (Barraclough et al. 2003) and are also given in Table 2. Fully calibrated hydrogen fluence measurements in *Genesis* targets are not yet available. The measured GIM H fluxes were distributed into the regime bins according to the regime selection algorithm. Proton measurements from the GIM are accurate to ±10%, which is typical of in situ electrostatic energy analyzer instruments. The 34% higher proton flux in the slow relative to the fast solar wind is in agreement with in situ measurements (Schwenn 1990; von Steiger et al. 2010).

GIM proton fluences were used together with our measured ^{4}He fluences to determine ^{4}He/H ratios for each solar wind regime. We did not consider He fluences measured by GIM because He flux measurements with electrostatic energy analyzers are prone to error, as alpha particles manifest themselves as a small peak on the shoulder of the main proton peak and can be difficult to resolve at low He abundances or hot plasma temperatures. We therefore rely only on He fluences derived from our target analyses, which were measured with high precision and accuracy. Diffusion experiments on a flight DOS target showed that He was quantitatively retained (Heber et al. 2009). Also, the number of protons trapped in the passive collectors is too low to cause radiation damages in DOS that probably would lead to substantial diffusion losses (Vainonen et al. 1997).

The ^{4}He/H is 0.0344 in the slow solar wind and 0.0406 in the fast solar wind (Table 2). The He/H ratios obtained for the slow and fast solar wind with *Genesis* are in agreement with He/H ratios measured in situ with the *WIND* spacecraft (Kasper et al.

2007) at the same period of the solar cycle when *Genesis* collected its solar wind, which was at and after solar maximum. Note that in contrast to in situ data that have a high resolution in solar wind speed, the *Genesis* H fluxes were distributed into the two speed bins of fast and slow solar wind, which results in reduced differences in the He/H.

5. DISCUSSION

5.1. Genesis Solar Wind Regime Data in Context with Literature Values

This is the first time isotopic fractionation between fast and slow solar wind has been unambiguously detected for elements heavier than helium. Our data show a clear depletion of the heavy isotopes in the slow solar wind for He, Ne, and Ar with the relative depletion decreasing with increasing elemental mass. Previous *Genesis* analyses on regime targets could not find such differences for Ne and Ar (Meshik et al. 2007; no He data available).

Differences in isotopic composition between fast and slow solar wind were known for He from measurements by the SWICS instrument on board the *Ulysses* spacecraft. These measurements pointed toward a depletion of ^{4}He over ^{3}He in the slow solar wind by about 100‰ relative to the fast solar wind (e.g., Bodmer & Bochsler 1998b; Gloeckler & Geiss 2000). Our data (63‰ for ^{3}He/^{4}He) are in agreement with the in situ data in both the sign and the magnitude of isotopic fractionation.

Both in situ studies used more diverse data sets of solar wind (including polar coronal holes, active and quiet periods of in-ecliptic solar wind) than has been sampled by *Genesis*. The larger fractionation displayed by the in situ data could also be related to the more strict separation by solar wind speed: only ions with speeds >700 km s^{-1} were included in the fast solar wind and ions at <500 km s^{-1} in the slow wind sample of *Ulysses*, respectively (Bodmer & Bochsler 1998b; Gloeckler & Geiss 2000). Furthermore, larger fluctuations in in situ data could also be caused by unaccounted uncertainties in counting statistics as ^{3}He is a relatively rare species. In contrast, *Genesis* collected solar wind ions that were faster than 525 km s^{-1} on the fast solar wind panel, ions slower than 425 km s^{-1} on the slow solar wind panel, and ions between 425 km s^{-1} and 525 km s^{-1} as either fast or slow wind, as explained above. The difference in collection strategies would tend to reduce

compositional differences between fast and slow regimes for *Genesis*, as seen in other parameters diagnostic of fast and slow solar wind (e.g., Reisenfeld et al. 2007). Isotopic fractionation was also observed for He in individual *Apollo* foil experiments (Geiss et al. 1972; Geiss et al. 2004). Although the *Apollo* foils did not discriminate between particular solar wind regimes, a correlation between He isotopic composition and the He/Ne ratio was observed (see review by Bochsler 2007a).

For elements heavier than helium in situ detection of differences in the isotopic composition between fast and slow solar wind was in most cases not successful. An exception is the combined analysis of Ne, Mg, and Si data obtained with the CELIAS/MTOF instrument on board the *Solar and Heliospheric Observatory* spacecraft for different solar wind speeds, for which Kallenbach et al. (1998b) found a depletion of the heavy isotopes by $14 \pm 13\permil$ amu^{-1} in the slow solar wind. Although with a large uncertainty, this result is basically in accordance with our finding. Uncertainties of the CELIAS/MTOF data are too large to determine the isotope fractionation for each element independently. All other studies investigating the isotopic compositions of single elements in fast and slow solar wind, respectively, e.g., Mg (Boschler et al. 1997) and Ar (Weygand et al. 2001), resulted in identical compositions within uncertainties. In general, the uncertainties often of $\geqslant 10\%$ (see review by Bochsler 2007a) prevent available in situ isotopic data to be useful in the geo- and cosmochemistry context. For example, even the ^{18}O/^{16}O composition between the Sun and typical planetary matter differs by less than some 7% (McKeegan et al. 2011); however, this is an extreme heterogeneity for planetary materials.

5.2. Isotopic Fractionation During Solar Wind Formation and Acceleration

Precise data for the bulk solar wind composition were obtained from *Genesis* samples, e.g., O (McKeegan et al. 2011), N (Marty et al. 2011), and noble gases (Meshik et al. 2007, 2009; Heber et al. 2009; Vogel et al. 2011b; Crowther & Gilmour 2012; Pepin et al. 2012). In order to obtain the solar nebula isotopic composition of these elements, which is the ultimate objective of the *Genesis* mission, the fractionation during solar wind formation and acceleration has to be corrected. The isotopic fractionation for elements up to mass 38 between slow and fast solar wind regimes reported in this work strongly implies that O and N are also isotopically fractionated in the solar wind relative to the composition of the OCZ, which is considered to be representative for solar nebula composition (Lodders et al. 2009) apart from the gravitational settling that could have increased the light isotope abundances in the OCZ over time by 3–4‰ amu^{-1} for O and N (Turcotte & Wimmer-Schweingruber 2002).

We test our data with respect to predictions of two available models that describe isotopic fractionation in the solar wind: the "correlation approach" (Gloeckler & Geiss 2000) and the "inefficient Coulomb drag" model (Bodmer & Bochsler 1998a, 2000). We do not consider here other hypotheses aiming to explain fractionation processes in the solar wind (e.g. Marsch et al. 1995; Wang 1996; Henoux 1998; Laming 2004, 2009) because so far these models have not attempted to predict isotopic fractionation. The inefficient Coulomb drag model and the correlation approach originally were both conceived to explain in situ data on He isotopes and abundances. Our goals here are to investigate whether these two models can explain our data on the isotopic fractionation between fast and slow solar wind and thus to quantify the fractionation between the solar
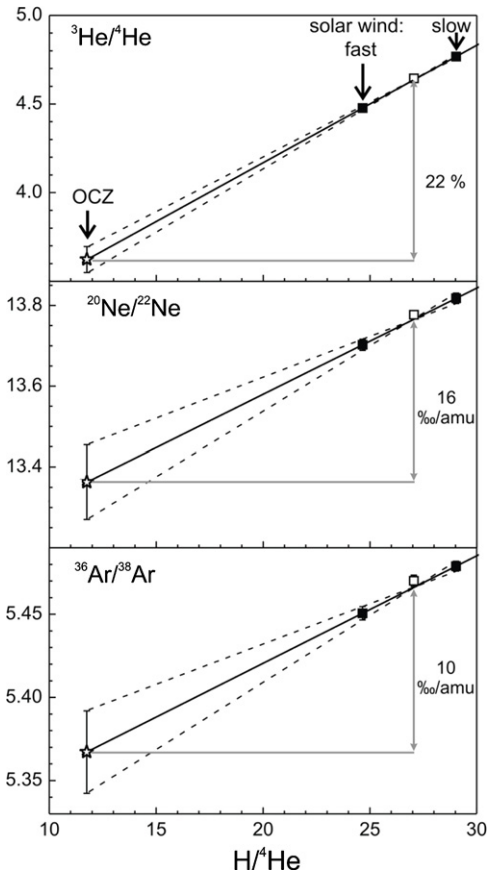
Figure 5. Correlation of He, Ne, and Ar isotopic ratios with H/He measured in slow and fast solar wind (filled squares) and extrapolated to the OCZ H/He composition (star) (11.75; Basu & Antia 2004) to deduce OCZ composition (according to Gloeckler & Geiss 2000). The given fractionation factor represents the difference between OCZ and bulk solar wind (open square; a fluence-weighted average of slow and fast solar wind H/He (=27.06) is used here representing the bulk solar wind without CME, see the text). The errors of the deduced photospheric isotopic compositions are 1σ.

wind and the OCZ for He, Ne, and Ar and other elements within this mass range.

Correlation approach. Gloeckler & Geiss (2000, hereafter GG2000) noted an empirical correlation of the mean ^{3}He/^{4}He composition of fast and slow solar wind with the respective Si/O as well as H/^{4}He ratios. They proposed a linear extrapolation to the photospheric Si/O and H/^{4}He compositions, respectively, to estimate the present-day He isotopic composition in the OCZ. This approach was based on the argument that the first ionization potential (FIP) imposes a fractionation between the Si and O abundances in the slow and fast solar wind and, based on the correlation, possibly also of the He/H and the ^{3}He/^{4}He ratios.

We apply the approach by GG2000 to our data. Fitting the fast and slow solar wind components (similar to GG2000) and extrapolating to the photospheric H/He ratio of 11.75 (Basu & Antia 2004), we obtain an ^{3}He/^{4}He ratio of the OCZ of $(3.62 \pm 0.07) \times 10^{-4}$ (Figure 5), a result in agreement with the OCZ composition estimated by GG2000 and Geiss & Gloeckler (2009) within uncertainties. We may extend this approach to calculate the OCZ Ne and Ar isotopic composition: ^{20}Ne/^{22}Ne = 13.36 ± 0.09; ^{36}Ar/^{38}Ar = 5.37 ± 0.03 (Figure 5, Table 5). The resulting overall isotopic fractionation factors between OCZ and bulk solar wind are 220‰ for He, 16‰ amu^{-1} for Ne, and 10‰ amu^{-1} for Ar. Except for He these numbers are similar

Table 5
Calculated Photospheric Compositions

| | ^{3}He/^{4}He | Total Fractionation OCZ – Bulk Solar Wind | ^{20}Ne/^{22}Ne | Total Fractionation OCZ – Bulk Solar Wind | ^{36}Ar/^{38}Ar | Total Fractionation OCZ – Bulk Solar Wind |
	($\times 10^{-4}$)	(‰)		(‰ amu^{-1})		(‰ amu^{-1})
Correlation approach	3.62	220	13.36	16	5.37	10
Entire He/H fractionation by inefficient Coulomb drag	3.12	488	13.34	16	5.31 (q = +9) 5.35 (q = +10)	11–15

Note. See the text for the procedure of calculation.

to those obtained by the inefficient Coulomb drag model (see below and Table 5).

However, we note that a physical model to explain this correlation is missing. It also seems unlikely that a purely atomic parameter such as FIP or first ionization time (FIT) could cause the observed variability of the helium isotopic ratio. A model of the FIP fractionation mechanism by Marsch et al. (1995) predicts negligible isotope fractionation upon ionization of the solar wind species, at maximum 16‰ for the ^{3}He/^{4}He ratio and $\leqslant 0.5‰$ amu^{-1} for Ne- and Ar-isotopic compositions. These small FIP/FIT isotopic fractionation factors are in contrast to (1) the measured He isotopic composition and the respective OCZ composition extrapolated by GG2000 and also (2) the variability of the He, Ne, and Ar isotopic composition between slow and fast solar wind measured in this work. Besides, we also remark on a missing self-consistency of the correlation as presented by GG2000. For example, GG2000 obtain a photospheric ^{3}He/^{4}He ratio of $\sim 3.75 \times 10^{-4}$ by extrapolating the measured ^{3}He/^{4}He and Si/O and H/He ratios, respectively, whereas an unreasonable low ^{3}He/^{4}He ratio of 7.1×10^{-5} would result from extrapolating the measured ^{3}He/^{4}He and Si/He ratios. Based on these arguments we prefer in the following the inefficient Coulomb drag model over the correlation approach to explain isotopic fractionation in the solar wind.

Inefficient Coulomb drag. The model of inefficient Coulomb drag (ICD) was developed to explain the observed low He/H and associated enhanced ^{3}He/^{4}He ratio in the slow solar wind relative to the fast solar wind composition (e.g., Bodmer & Bochsler 1998a, 2000).

In slow solar wind, proton drag is thought to be a dominant acceleration mechanism by Bürgi & Geiss (1986), whereas wave particle interaction can only play a minor role, as is evidenced in kinetic properties of minor species as far out as 1 AU (e.g., Hefti et al. 1998). However, due to the rapid expansion of flux tubes in the coupling region and the concomitant rapidly decreasing proton density, the drag is considered to become inefficient, and—in the absence of efficient wave pressure—heavy species can become strongly depleted relative to protons. In situ measurements show that in particular ^{4}He^{2+} is preferentially depleted relative to hydrogen because of its exceptionally unfavorable Coulomb drag factor (see below). This concept also implies a mass-dependent isotope fractionation resulting in a depletion of heavier isotopes in the slow solar wind. In contrast, wave particle interaction plays a major role in heating and accelerating heavy species in the fast, coronal hole associated solar wind (e.g., Cranmer & van Ballegooijen 2012). In this type of solar wind regime Coulomb drag seems to play a minor role, at least outside the chromosphere. There is evidence for the importance of wave heating and wave acceleration in fast solar wind from many optical observations and in situ studies. Since wave action is not expected to strongly discriminate between

different isotopic species (Bochsler 2000), low-mass species are not strongly enhanced over heavier species in fast solar wind. Similarly, ^{4}He^{2+} seems least depleted in the fast solar wind and thus isotopic composition of the fast solar wind should at best be only slightly mass fractionated relative to OCZ compositions (e.g., Wimmer-Schweingruber 2002).

Here we discuss mass fractionation between slow and fast solar wind in more detail and use the ICD model to deduce photospheric isotopic compositions of He, Ne, and Ar. Finally, implications for solar nebula oxygen and nitrogen isotopic compositions based on recently measured bulk solar wind (Marty et al. 2011; McKeegan et al. 2011) are discussed.

We first test the ICD model by comparing the measured isotopic fractionations of noble gases between fast and slow solar wind with model predictions. Following the equations derived by Bodmer & Bochsler (1998a, 2000) and Grimberg et al. (2008), we calculate the fractionation factor f of two isotopes i, j of the same element as function of the ^{4}He/H fractionation between the slow and the fast solar wind:

$$f_{i,j} = \frac{(H_{^4\mathrm{He}} - H_i) + f_{^4\mathrm{He/H}} * H_i}{(H_{^4\mathrm{He}} - H_j) + f_{^4\mathrm{He/H}} * H_j}. \quad (2)$$

Here, $f_{^4\mathrm{He/H}}$ is the ratio of ^{4}He/H in the slow divided by that in the fast solar wind (thus $f_{^4\mathrm{He/H}}$ is 1 for fast solar wind). The Coulomb drag factor H for different isotopes defines the ordering according to their velocities and thus for predicted fractionation factors and is based on their mass A and the charge state Q of the respective element:

$$H_i = \frac{2A_i - Q_i - 1}{Q_i^2} \sqrt{\frac{A_i + 1}{A_i}}. \quad (3)$$

It is generally assumed that the charge state distribution is, to a good approximation, the same for all isotopes of an element (R. Leske 2010, private communication).

The charge state of the element is an important parameter in this equation as it affects the extent of the isotopic fractionation. Charge state distributions measured in situ for He and Ne exhibit mean values of $+2$ and $+8$ (Gloeckler & Geiss 2007), respectively. Unlike He and Ne, the assumed charge state distribution of Ar relies entirely on model calculations (e.g., Bochsler 2000; Figure 6). Accordingly, at 1 AU the dominant charge state is $+9$ (Figure 6). The process of proton coupling, however, is presumed to only operate within the inner corona, <3 solar radii and Figure 6 suggests Ar^{10+} as the average charge state in this region. The same type of model predicts that He and Ne charge states are established within 1 and 1.1 solar radii and remain constant farther out (Bochsler 2007b). We therefore adopt the He and Ne charge states measured at $\geqslant 1$ AU and provide isotopic fractionation factors for Ar^{9+} and Ar^{10+} in the
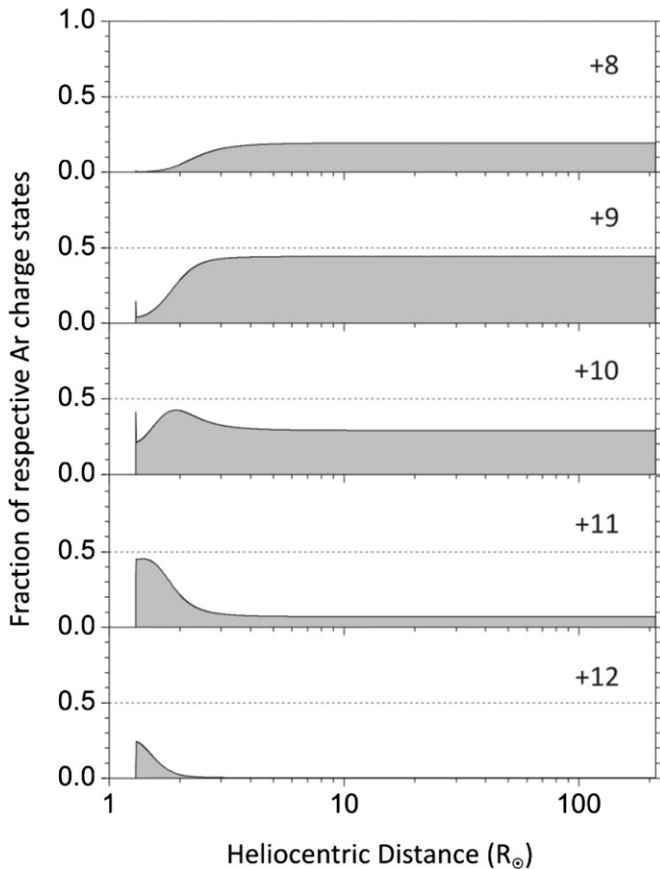
Figure 6. Evolution of charge states of Ar as a function of the heliocentric distance in solar radii. 1 AU is at $216 R_{\odot}$. The charge state balance of Ar was calculated using the ionization and recombination rates given by Arnaud & Rothenflug (1985) and a simple, Parker-type, radially expanding solar wind acceleration model (Bochsler 2000). The conditions can be considered as typical for slow solar wind (coronal temperature maximum at 2.1 MK, solar wind speed at 1 AU of 438 km s^{-1}). The same model reproduces the iron charge states typically observed in slow solar wind (e.g., Aellig et al. 1997).

following. Generally, except for He, charge states are slightly lower in the fast wind than in the slow wind. Mean charge states measured on *ACE* differ by 2% for Ne and <10% for heavier ions such as Si and Fe (no data available for Ar; Landi et al. 2012). These differences have, however, a negligible effect on the amount of fractionation predicted by the ICD.

The calculated mass fractionation factors between slow and fast solar wind based on the ICD model (in comparison to the measured ones in parentheses) are for He: 67‰ (63 ± 2‰), Ne: 3.6‰ amu^{-1} (4.2 ± 0.4‰ amu^{-1}), and Ar: 2.9‰ amu^{-1} ($q = +9$), 2.3‰ amu^{-1} ($q = +10$) (2.6 ± 0.5‰ amu^{-1}). In each case, the predicted isotopic fractionation is in good agreement with the measured data in sign and magnitude. Furthermore, in agreement with the measured Ne data (Figure 4), the model predicts a mass-dependent isotopic fractionation. Data and model also agree in the decreasing extent of isotopic fractionation with increasing atomic mass (see Bürgi & Geiss 1986; Bodmer & Bochsler 2000). The measured heavy element depletion in the slow solar wind with respect to protons and fast solar wind is also essentially in accordance with predictions by the ICD model. Measured depletions amount to between 15% and 18% for He/H, Ne/H, and Ar/H, whereas modeled depletions are in the same direction but larger, ranging between 25% and 70% depending on model assumptions (Bodmer & Bochsler 2000). However, data and ICD model predictions disagree with respect

to the elemental fractionation between slow and fast solar wind among the heavy ions themselves. Bochsler (2007a) explained a ∼300‰ difference in the ^{4}He/^{20}Ne ratio measured in two different aluminum foils exposed during the *Apollo* Solar Wind Composition experiment as being due to ICD fractionation. Our samples of slow and fast solar wind, however, show the same ^{4}He/^{20}Ne ratio within 20‰ and, relative to Ar and fast solar wind, the slow solar wind is even enriched in He by 40‰, contrary to the ICD model prediction.

Overall, the inefficient Coulomb drag model appears to successfully explain isotopic fractionation between the slow and fast solar wind. However, the predicted strong He depletion relative to heavier ions in the slow solar wind is not observed. We will thus only discuss our isotope data and the He depletion relative to H in the framework of this model.

The He/H ratio and its importance on the derivation of OCZ isotopic composition. The He/H ratio is predicted to be an important parameter associated with isotopic fractionation by both the inefficient Coulomb drag model and the correlation method (see above). As can be seen in Equation (2), the extent of isotopic fractionation predicted by the ICD model depends on the He/H fractionation. Besides the different He/H compositions in fast and slow solar wind, which probably can be explained by processes described above, the reason for the overall He depletion of about a factor of two from photospheric to coronal composition is not entirely understood. Such an understanding will be required for a reliable derivation of OCZ isotopic composition from solar wind data.

Several researchers ascribe the overall depletion of He relative to H in the corona to differences in ionization efficiencies of the two species, e.g., due to ion-neutral separation in the upper chromosphere or transition region (Geiss 1982; von Steiger & Geiss 1989; Marsch et al. 1995). Considering only this effect, the predicted associated isotopic fractionations are at most 16‰ for ^{3}He/^{4}He, 0.5‰ amu^{-1} for Ne, and 0.2‰ amu^{-1} for Ar (Marsch et al. 1995) and can thus be considered negligible here. If so, the isotopic composition in the fast solar wind of ^{3}He/^{4}He (4.48×10^{-4}), ^{20}Ne/^{22}Ne (13.70), and ^{36}Ar/^{38}Ar (5.45) measured in this work would be quite representative for the OCZ composition (Table 2). On the other hand, Bochsler et al. (2006) argued on the basis of a correlation between in situ measured He/H and O/H ratios that inefficient Coulomb drag is the main process responsible for the He/H fractionation between photospheric and coronal composition and not just for the regime-related variation of the He abundance. If the latter is the case, a considerable isotopic fractionation of solar wind relative to OCZ composition is expected.

Isotopic fractionation between the Sun and solar wind. In this section we apply the ICD model to our measured data, assuming that ICD is responsible for the overall fractionation of the He/H between photosphere and corona, and calculate the isotopic composition of He, Ne, and Ar in the OCZ. The fractionation of two isotopes of the same element is calculated as above (Equations (2) and (3)) adopting for $f_{^4\text{He}/\text{H}}$ the ratio of ^{4}He/H in the bulk solar wind without CME of 0.0370 (see above) and photospheric He/H of 0.085 (Basu & Antia 2004). The resulting fractionation factors and isotopic composition of the OCZ are for ^{3}He/^{4}He 488‰ and 3.12×10^{-4}, for ^{20}Ne/^{22}Ne 16‰ amu^{-1} and 13.34. The respective values for ^{36}Ar/^{38}Ar are 11–15‰ amu^{-1} and 5.35–5.31, depending on whether charge state $+10$ or $+9$ is assumed for Ar (Table 5). Our inferred values for the ^{3}He/^{4}He and ^{20}Ne/^{22}Ne composition of the OCZ are in agreement with respective values given by

Bodmer & Bochsler (1998a) and Bochsler (2007b). Generally, the ICD model results in similar heavy isotopic compositions of the OCZ relative to solar wind for the medium-mass elements Ne and Ar as the correlation approach, with exception of He which is ∼14% heavier with the former method.

We can also attempt to evaluate the extent of isotopic fractionation between solar wind and OCZ by comparing oxygen and nitrogen data obtained by *Genesis* with adopted solar nebula values as derived from meteorite data. The $\delta^{18}O$ composition of the bulk solar wind measured in the *Genesis* concentrator target is −99‰ relative to SMOW (Equation (1): $R = {}^{18}O/{}^{16}O$, $R_{standard}$ = SMOW (standard mean ocean water); McKeegan et al. 2011). If ICD is solely responsible for solar wind isotopic fractionation, and if this fractionation is linearly mass dependent as indicated by our Ne isotope data, the data points representing the measured solar wind composition and the true solar composition should fall on a mass-dependent fractionation line with slope of 0.52 in the oxygen three-isotope plot (McKeegan et al. 2011). The solar wind composition plots to the left (low-mass) side of the CCAM (Carbonaceous chondrite anhydrous minerals) line, the dominant ${}^{16}O$-mixing line for refractory solar nebula materials. McKeegan et al. (2011) and Heber and McKeegan (2011) interpreted the intersection of the mass fractionation line through solar wind composition with the CCAM line as being the true average initial O isotopic composition of the solar nebula. This hypothesis would mean that O isotopes in the solar wind are fractionated by about 22‰ amu^{-1} toward a lighter composition. The amount of O isotopic fractionation predicted by the ICD model is 31‰ amu^{-1} in this same direction, using the mean charge state of O of +6 in the bulk solar wind (Landi et al. 2012) and the measured bulk solar wind He/H of 0.0402. We use the measured bulk solar wind He/H (that includes the CME portion) because the O data were obtained from a bulk solar wind collector and nothing is known so far about the O isotopic composition of the CME-related solar wind. An He/H ratio of 0.037 (bulk solar wind without the CME portion) would lead to a slightly higher predicted fractionation of 34‰ amu^{-1}. In any case, predicted and observed O fractionations are in reasonable agreement with each other considering other sources of uncertainties as, e.g., the unknown charge state distribution of O in the solar wind acceleration region.

The N isotopic composition measured in the bulk solar wind in the *Genesis* concentrator target ($\delta^{15}N$ = −407‰; Marty et al. 2011) (Equation (1): $R = {}^{15}N/{}^{14}N$, $R_{standard}$ = ATM (terrestrial atmosphere)) can be compared with N measured in osbornite ($\delta^{15}N$ = −358‰; Meibom et al. 2007), a high temperature condensate embedded in a calcium–aluminum-rich inclusion (CAI) considered to represent the unfractionated N isotopic composition of the gas phase of the early solar nebula. This comparison hints at a mass fractionation between solar wind and the Sun of 49‰. The fractionation predicted by the ICD model is about 48‰ (using the major charge state of N of +5 and the He/H ratio of 0.0402). Thus, as with oxygen, the magnitude and sign of isotopic mass fractionation between solar wind and the Sun inferred via *Genesis* and meteorite data and that predicted by the ICD model agree well with each other.

The good agreement between observed and predicted mass fractionation for O, N and He, and Ne and Ar gives confidence that the inefficient Coulomb drag model can be used to derive OCZ or solar nebula isotopic abundances from measured solar wind isotopic data. However, more theoretical and analytical work is required to better understand isotopic fractionation

processes upon solar wind formation and acceleration in general and in particular the behavior of He relative to H, i.e., whether isotopic fractionation in the solar wind is indeed closely related to the He/H fractionation. Independent tests of the inefficient Coulomb drag model may be provided by isotopic measurements of non-volatile elements. Initial data are likely to be provided by the Mg isotopic composition in *Genesis* targets (Heber et al. 2012). The Mg isotopic composition of known terrestrial and extraterrestrial solids (except in CAI's) is identical within 1‰ (Young & Galy 2004), thus an agreement with solar photosphere composition is expected, assuming no gravitational separation within the Sun over its 4.5 Ga life. If gravitational settling took place, the photospheric Mg isotopic composition were 1–2‰ amu^{-1} lighter than the chondritic composition (Turcotte & Wimmer-Schweingruber 2002). A precision better than about 10‰ is required for the *Genesis* measurement to be able to detect the potential fractionation of the solar wind Mg isotopic composition since the Coulomb drag model predicts a depletion of ${}^{26}Mg$ over ${}^{24}Mg$ of 23‰. Preliminary data tend to support a lighter isotopic composition of the solar wind (Heber et al. 2012).

6. CONCLUSIONS

The elemental and the isotopic compositions of He, Ne, and Ar were measured in the fast and slow solar wind regimes collected separately on the *Genesis* spacecraft. We find clear differences in the isotopic composition for all three elements between slow and fast solar wind using a very precise analytical technique. Heavy isotopes are depleted in the slow solar wind compared to the fast wind, by 63‰ for He, 4.2‰ amu^{-1} for Ne, and 2.6‰ amu^{-1} for Ar. Based on the three Ne isotopes, we conclude that the fractionation process is mass dependent. Our results are in line with the He data measured in situ and clearly point to isotopic fractionation processes taking place upon solar wind formation. The inefficient Coulomb drag model appears to successfully explain the measured isotopic fractionation between fast and slow solar wind. However, data and model disagree with respect to elemental fractionation among the heavy ions. Our data show no depletion but possibly a slight enrichment of He relative to Ne and Ar in the slow solar wind compared to the fast, which is opposite to ICD model that predicts He depletion.

The differences in the isotopic composition of O and N between the measured solar wind and early solar system condensates, probably representing solar nebula composition, also suggest that the solar wind is isotopically mass fractionated. The magnitude and sign of the observed differences are in good agreement with the predicted isotopic fractionation based on the ICD model for both elements. An open question affecting the results of the ICD, as well as the correlation method, concerns the actual cause of the overall He/H fractionation between photospheric and solar wind composition. Partially associated is the question of whether the isotopic fractionation is entirely or only partially tied to the He/H fractionation. Future analyses of the isotopic composition of the non-volatile element Mg in solar wind samples in comparison to the terrestrial Mg isotopic composition will provide further constraints on the nature of isotopic mass fractionation upon solar wind formation.

REFERENCES

Aellig, M. R., Grünwaldt, H., Bochsler, P., et al. 1997, in 31st ESLAB Symp., Correlated Phenomena at the Sun, in the Heliosphere and in Geospace, ed. A. Wilson (ESA SP-415; Noordwijk: ESTEC), 27
Albarède, F., & Beard, B. 2004, in Reviews in Mineralogy and Geochemistry, Vol. 55, ed. C. M. Johnson, B. Beard, & F. Albarède (Washington, DC: Mineralogical Society of America), 113
Arnaud, M., & Rothenflug, R. 1985, A&AS, 60, 425
Asplund, M., Grevesse, N., Sauval, A. J., & Scott, P. 2009, ARA&A, 47, 481
Barraclough, B. L., Dors, E. E., Abeyta, R. A., et al. 2003, Space Sci. Rev., 105, 627
Basu, S., & Antia, H. M. 2004, ApJ, 606, L85
Baur, H. 1980, PhD Thesis, ETH Zürich
Baur, H. 1999, EOS Trans. Am. Geophys. Union, 46, F1118
Bochsler, P. 2000, Rev. Geophys., 38, 247
Bochsler, P. 2007a, A&AR, 14, 1
Bochsler, P. 2007b, A&A, 471, 315
Bochsler, P., Auchère, F., & Skoug, R. M. 2006, in SOHO-17, ed. H. Lacoste & L. Ouwehand (ESA SP-617; Giardini Naxos, Italy), CD 28.1
Boschler, P., Balsiger, H., Bodmer, R., et al. 1997, Phys. Chem. Earth, 22, 401
Bodmer, R., & Bochsler, P. 1998a, Phys. Chem. Earth, 23, 683
Bodmer, R., & Bochsler, P. 1998b, A&A, 337, 921
Bodmer, R., & Bochsler, P. 2000, J. Geophys. Res., 105, 47
Bürgi, A., & Geiss, J. 1986, Sol. Phys., 103, 347
Burnett, D. S., Barraclough, B. L., Bennett, R., et al. 2003, Space Sci. Rev., 105, 509
Burnett, D. S., & Team, G. S. 2011, Proc. Natl. Acad. Sci., 108, 19147
Clayton, R. N. 2003, in Treatise in Geochemistry, ed. A. M. Davis (Oxford: Elsevier), 129
Cranmer, S. R., & van Ballegooijen, A. A. 2012, ApJ, 754, 92
Crowther, S. A., & Gilmour, J. D. 2012, J. Anal. At. Spectrom., 27, 256
Geiss, J. 1982, Space Sci. Rev., 33, 201
Geiss, J., Buehler, F., Cerutti, H., Eberhardt, P., & Filleux, C. H. 1972, in Apollo-16 Preliminary Science Report (NASA-SP), 14/1
Geiss, J., Bühler, F., Cerutti, H., et al. 2004, Space Sci. Rev., 110, 307
Geiss, J., & Gloeckler, G. 2009, in IAU Symp. 268, Light Elements in the Universe, ed. C. Charbonnel, M. Tosi, F. Primas, & C. Chiappini (Cambridge: Cambridge Univ. Press), 71
Geiss, J., & Reeves, H. 1972, A&A, 18, 126
Gloeckler, G., & Geiss, J. 2000, in IAU Symp. 198, The Light Elements and Their Evolution, ed. L. da Silva, M. Spite, & J. R. de Medeiros (Cambridge: Cambridge Univ. Press), 224 (GG2000)
Gloeckler, G., & Geiss, J. 2007, Space Sci. Rev., 130, 139
Grimberg, A., Baur, H., Bühler, F., Bochsler, P., & Wieler, R. 2008, Geochim. Cosmochim. Acta, 72, 626
Heber, V. S., Baur, H., Bochsler, P., et al. 2008, in 39th LPSC, No. 1391, 1779
Heber, V. S., Jurewicz, A. J. G., Janney, P., et al. 2012, 43rd LPSC, No. 1659, 2921
Heber, V. S., & McKeegan, K. D. 2011, in 42nd LPSC, No. 1608, 2789

Heber, V. S., Wieler, R., Baur, H., Olinger, C. T., & Burnett, D. S. 2009, Geochim. Cosmochim. Acta, 73, 7414
Heber, V. S., Wiens, R. C., Jurewicz, A. J. G., et al. 2011, Meteorit. Planet. Sci., 46, 493
Hefti, S., Grünwaldt, H., Ipavich, F. M., et al. 1998, J. Geophys. Res., 103, 29697
Henoux, J.-C. 1998, Space Sci. Rev., 85, 215
Jurewicz, A. J. G., Burnett, D. S., Wiens, R. C., et al. 2003, Space Sci. Rev., 105, 535
Kallenbach, R., Ipavich, F. M., Bochsler, P., et al. 1998a, ApJ, 498, L75
Kallenbach, R., Ipavich, F. M., Kucharek, H., et al. 1998b, Space Sci. Rev., 85, 357
Karrer, R., Bochsler, P., Giammanco, C., et al. 2007, Space Sci. Rev., 130, 317
Kasper, J. C., Stevens, M. L., Lazarus, A. J., Steinberg, J. T., & Ogilvie, K. W. 2007, ApJ, 660, 901
Laming, J. M. 2004, ApJ, 614, 1063
Laming, J. M. 2009, ApJ, 695, 954
Landi, E., Gruesbeck, J. R., Lepri, S. T., & Zurbuchen, T. H. 2012, ApJ, 758, L21
Liu, M. C., McKeegan, K. D., Goswami, J. N., et al. 2009, Geochim. Cosmochim. Acta, 73, 5051
Lodders, K., Palme, H., & Gail, H. P. 2009, in Landolt-Börnstein, Group VI: Astronomy and Astrophysics (Berlin: Springer), 560
Marsch, E., von Steiger, R., & Bochsler, P. 1995, A&A, 301, 261
Marty, B., Chaussidon, M., Wiens, R. C., Jurewicz, A. J. G., & Burnett, D. S. 2011, Science, 332, 1533
McKeegan, K. D., Kallio, A. P. A., Heber, V. S., et al. 2011, Science, 332, 1528
Meibom, A., Krot, A. N., Robert, F., et al. 2007, ApJ, 656, L33
Meshik, A., Hohenberg, C., Pravdivtseva, O., et al. 2009, in 40th LPSC, 2037
Meshik, A. P., Mabry, J., Hohenberg, C., et al. 2007, Science, 318, 433
Neugebauer, M., Steinberg, J. T., Tokar, R. L., et al. 2003, Space Sci. Rev., 105, 661
Pepin, R. O., Schlutter, D. J., Becker, R. H., & Reisenfeld, D. B. 2012, Geochim. Cosmochim. Acta, 89, 62
Reisenfeld, D. B., Burnett, D. S., Becker, R. H., et al. 2007, Space Sci. Rev., 130, 79
Schwenn, R. 1990, in Physics of the Inner Heliosphere I, ed. R. Schwenn & E. Marsch (Berlin: Springer), 99
Shamsa, M., Liu, W. L., Balandin, A. A., et al. 2006, Appl. Phys. Lett., 89, 161921
Turcotte, S., & Wimmer-Schweingruber, R. F. 2002, J. Geophys. Res., 107, 1442
Vainonen, E., Likonen, J., Ahlgreen, T., Haussalo, P., & Keinonen, J. 1997, J. Appl. Phys., 82, 3791
Vogel, N., Baur, H., Burnett, D. S., Maden, C., & Wieler, R. 2011a, in 42nd LPSC, No. 1608, 1767
Vogel, N., Heber, V. S., Baur, H., Burnett, D. S., & Wieler, R. 2011b, Geochim. Cosmochim. Acta, 75, 3057
von Steiger, R, & Geiss, J. 1989, A&A, 225, 222
von Steiger, R., Zurbuchen, T. H., & McComas, D. J. 2010, Geophys. Res. Lett., 37, L22101
Wang, Y. M. 1996, ApJ, 464, L91
Weygand, J. M., Ipavich, F. M., Wurz, P., Paquette, J., & Bochsler, P. 2001, Geochim. Cosmochim. Acta, 65, 4589
Wimmer-Schweingruber, R. F. 2002, Adv. Space Res., 30, 23
Wimmer-Schweingruber, R. F., Bochsler, P., Kern, O., Gloeckler, G., & Hamilton, D. C. 1998, J. Geophys. Res., 103, 20621
Wurz, P., Bochsler, P., & Lee, M. A. 2000, J. Geophys. Res., 105, 27239
Young, E. D., & Galy, A. 2004, in Geochemistry of Non-Traditional Stable Isotopes, ed. C. M. Johnson, B. Beard, & F. Albarède, 197
Ziegler, J. F. 2004, Nucl. Instrum. Methods Phys. Res., 219/220, 1027
Zurbuchen, T. H., Fisk, L. A., Lepri, S. T., & von Steiger, R. 2003, in AIP Conf. Proc. 679, Solar Wind Ten, ed. M. Velli, F. Malara, & R. Bruno (Melville, NY: AIP), 604